Journal of Fluids and Structures (1995) **9**, 175–193

THE AEROELASTIC RESPONSE OF A TWO-DIMENSIONAL AIRFOIL WITH BILINEAR AND CUBIC STRUCTURAL NONLINEARITIES

S. J. PRICE AND H. ALIGHANBARI
Department of Mechanical Engineering, McGill University
Montreal, Québec, H3A 2K6, Canada

AND

B. H. K. LEE
Institute for Aerospace Research, National Research Council
Ottawa, Ontario, K1A 0R6, Canada

(Received 13 June 1994 and in revised form 15 September 1994)

A two-dimensional airfoil with either a bilinear or cubic structural nonlinearity in pitch, and subject to incompressible flow has been analysed; the aerodynamic forces on the airfoil are evaluated using Wagner's function. The resulting equations are either integrated numerically using a finite difference method to give time histories of the airfoil motion, or solved in a semi-analytical manner using a dual-input describing function technique. For both types of nonlinearity regions of limit cycle oscillation (LCO) are detected for velocities well below the divergent flutter boundary. Using the finite difference method it is shown that the existence of the LCOs is strongly dependent on the initial conditions of the airfoil. Although the describing function method cannot predict the effect of initial conditions, it does give reasonable predictions of the velocity at which LCOs commence, and good predictions of the magnitude of the LCOs—at least for those cases where the LCO motion is predominantly period-one. The existence of the LCOs is strongly dependent on the properties of the airfoil. In some cases, most notably those with small structural preloads, regions of chaotic motion are obtained, as suggested by power spectral densities, phase-plane plots and Poincaré sections of the airfoil time histories; the existence of chaos was confirmed for the cubic nonlinearity via calculation of the Lyapunov exponents, one of which is positive. The fact that chaotic motion is obtained with both bilinear and cubic nonlinearities suggests that it is not the discontinuous nature of the stiffness, associated with the bilinear nonlinearity, which is responsible for producing this chaotic motion.

1. INTRODUCTION

THERE ARE MANY EXAMPLES OF NONLINEARITIES in the dynamics of aircraft structures which can have a significant effect on the aeroelastic response of the aircraft. An excellent review of some possible structural nonlinearities and their effect on aeroelastically induced vibrations is given by Brietbach (1977), and both structural and aerodynamic nonlinearities are considered by Dowell & Ilgamov (1988).

Structural nonlinearities may occur in either a distributed or concentrated form. However, in general, distributed nonlinearities only become appreciable for large amplitude vibrations, while concentrated nonlinearities can have a significant effect even for small vibrational amplitudes. Loose or worn hinges for control surfaces are one example of a concentrated structural nonlinearity which can lead to a limit cycle oscillation, LCO. An example of such an LCO for the CF-18 aircraft is given by Lee &

0889-9746/95/020175 + 19 $08.00

Tron (1989), who also show that loose control surfaces can be adequately represented via either a bilinear spring stiffness or a cubic nonlinearity. As reviewed recently by the present authors (Price *et al.* 1993), many authors have investigated the aeroelastic response of an airfoil with bilinear nonlinearities in either the plunge or pitch directions.

The present authors (Price *et al.* 1993) recently conducted a comprehensive investigation of the aeroelastic response of a two-dimensional airfoil with a free-play structural nonlinearity in pitch—this work was a continuation of that initiated by Lee & Desrochers (1987). The equations of motion were analysed using a finite difference method with the particular aim of examining the sensitivity of the airfoil aeroelastic response to its initial conditions. Possibly the conclusion of most practical importance from this work was that LCOs can occur for velocities well below the linear flutter boundary, which was in agreement with the numerical predictions of McIntosh *et al.* (1981) and Yang & Zhao (1988). The existence of these LCOs was strongly dependent on the airfoil initial conditions and, furthermore, it was shown that the "basin of attraction" for the LCO motion was a very complex five-dimensional shape in terms of the free-stream velocity and the airfoil initial pitch and plunge displacements, as well as their associated velocities. It was also suggested, via the use of phase-plane maps, Poincaré sections, bifurcation diagrams and spectral analysis, that the airfoil motion could be chaotic for a narrow range of airfoil parameters; chaos had also previously been suggested by a number of other authors (Hauenstein *et al.* 1990, 1992; Zhao & Yang 1990; Tang & Dowell 1992a). However, contrary to previously published results (Hauenstein *et al.* 1992) where it had been suggested that chaos was only possible with nonlinearities in both the pitch and plunge directions, chaotic motion was shown to be possible with a single structural nonlinearity in pitch. However, chaos was detected only for specific airfoil parameters, and was confined to small regions in the stability boundary diagram.

Following on from their previous analysis of a free-play nonlinearity (Price *et al.* 1993), the work presented here considers the aeroelastic response of an airfoil with either a bilinear or a cubic structural nonlinearity in pitch. As in the previous paper, the analysis is for a two-dimensional airfoil in incompressible flow. However, the airfoil motion is not only analysed via the finite difference method but also the describing function technique. Both methods of analysis indicate the presence of LCOs for velocities less than the linear flutter boundary. Furthermore, using the finite difference method it is demonstrated that, as in the case of the free-play nonlinearity, the occurrence of this LCO motion is strongly dependent on the airfoil initial conditions. It is also shown that, for a narrow range of structural parameters, chaotic motion can occur for both the cubic and bilinear nonlinearities.

A similar analysis to the one presented here was undertaken by Zhao & Yang (1990). They also investigated the dynamic response of a two-dimensional airfoil in incompressible flow with a cubic restoring moment in pitch, and used both a describing function technique (referred to by them as "equivalent linearization") and a time marching method—in their case Runge–Kutta numerical integration was employed. However, one big difference between the two analyses is the manner in which the aerodynamic forces are represented. As shown in the next section, the aerodynamic forces for the present investigation are obtained from a complete unsteady analysis using Wagner's function. Zhao & Yang (1990), however, limited themselves to a quasi-static analysis, where the lift and pitching moment depend only on the instantaneous pitch angle. As discussed in Section 3 of this paper, this difference in aerodynamics has a considerable effect on the dynamic response of the airfoil.

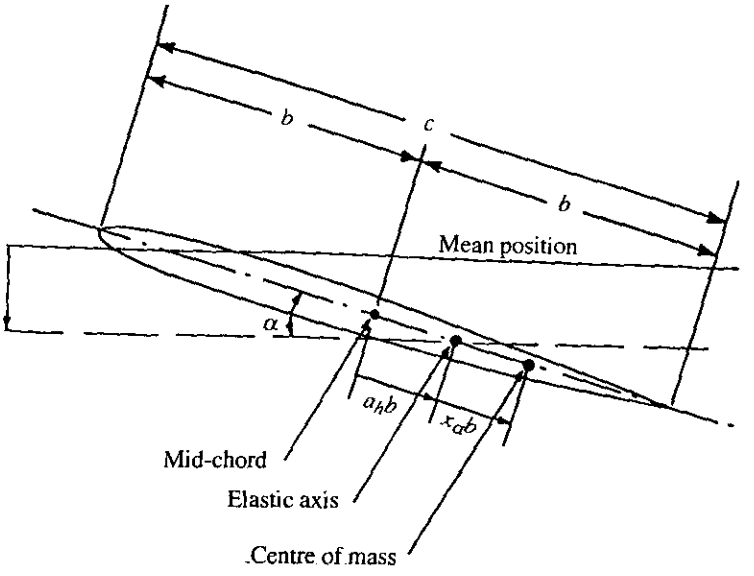

Figure 1. Schematic representation of the two-degree-of-degree freedom airfoil.

2. THEORETICAL ANALYSIS

As shown previously by the authors (Price *et al.* 1993), the equations of motion for the airfoil shown in Figure 1 may be written in nondimensional form as

$$\begin{aligned} \xi''(\tau) + x_\alpha \alpha''(\tau) + (2\zeta_\xi \bar{\omega}/U)\xi'(\tau) + (\bar{\omega}/U)^2 \xi(\tau) &= p(\tau), \\ (x_\alpha / r_\alpha^2)\xi''(\tau) + \alpha''(\tau) + (2\zeta_\alpha / U)\alpha'(\tau) + M(\alpha)/U^2 &= r(\tau), \end{aligned} \tag{1}$$

where α and ξ are the nondimensional pitch and plunge displacements of the elastic axis, respectively, $p(\tau)$ and $r(\tau)$ are the nondimensional force and moment, respectively, $M(\alpha)$ is the structural nonlinearity in pitch normalized with respect to the linear torsional stiffness [in the case of a linear system $M(\alpha)$ is simply α], $\bar{\omega}$ is the frequency ratio, ω_ξ/ω_α, U is the nondimensional air-speed, $V/b\omega_\alpha$, and the other symbols are defined in Appendix B.

For incompressible flow, $p(\tau)$ and $r(\tau)$ may be obtained [see, for example, Fung (1955)] for any arbitrary small-amplitude motion in terms of the airfoil initial conditions and Wagner's function, $\phi(\tau)$, giving

$$\begin{aligned} p(\tau) = -\frac{1}{\mu}\{\xi''(\tau) - a_h \alpha''(\tau) + \alpha'(\tau)\} - \frac{2}{\mu}\Big[\{\alpha(0) + \xi'(0) + \bar{a}_h \alpha'(0)\}\phi(\tau) \\ + \int_0^\tau \phi(\tau - \sigma)\{\alpha'(\sigma) + \xi''(\sigma) + \bar{a}_h \alpha''(\sigma)\}\, \mathrm{d}\sigma\Big], \end{aligned} \tag{2}$$

and

$$\begin{aligned} r(\tau) = \frac{2}{\mu r_\alpha^2}(1/2 + a_h)\Big[\{\alpha(0) + \xi'(0) + \bar{a}_h \alpha'(0)\}\phi(\tau) \\ + \int_0^\tau \phi(\tau - \sigma)\{\alpha'(\sigma) + \xi''(\sigma) + \bar{a}_h \alpha''(\tau)\}\, \mathrm{d}\sigma\Big] \\ + \frac{1}{\mu r_\alpha^2}[a_h\{\xi''(\tau) - a_h \alpha''(\tau)\} - \bar{a}_h \alpha'(\tau) - 1/8\alpha''(\tau)], \end{aligned} \tag{3}$$

where $\bar{a}_h = (\frac{1}{2} - a_h)$, $\phi(\tau) = l - ae^{-b\tau} - ce^{-d\tau}$, $l = 1$, $a = 0{\cdot}165$, $b = 0{\cdot}0455$, $c = 0{\cdot}335$ and $d = 0{\cdot}3$.

The specific structural nonlinearities considered are bilinear and cubic restoring moments in the pitch direction, as shown schematically in Figure 2. Using the notation given in Figure 2(a), $M(\alpha)$ for the bilinear stiffness is given by

$$M_\alpha = \begin{cases} M_0 + \alpha - \alpha_f, & \text{for } \alpha < \alpha_f, \\ M_0 + M_f(\alpha - \alpha_f), & \text{for } \alpha_f \leq \alpha \leq \alpha_f + \delta, \\ M_0 + \alpha - \alpha_f + \delta(M_f - 1) & \text{for } \alpha_f + \delta < \alpha, \end{cases} \tag{4}$$

and for the cubic nonlinearity, $M(\alpha)$, is given by

$$M(\alpha) = \beta_0 + \beta_1\alpha + \beta_2\alpha^2 + \beta_3\alpha^3. \tag{5}$$

To solve the above equations both the finite difference and describing function methods were employed as discussed in the following sections.

2.1. Finite Difference Method

In common with the authors' previous paper (Price *et al.* 1993), Houbolt's finite difference method (1950) was employed to solve the equations of motion.

For the airfoil with a bilinear stiffness equations (1) are rewritten, after considerable algebra, as

$$\begin{aligned} \bar{P}_{11}\alpha(\tau + \Delta\tau) + \bar{P}_{12}\xi(\tau + \Delta\tau) &= \bar{X}_1 \\ [\bar{P}_{21} + U^{-2}M_p]\alpha(\tau + \Delta\tau) + \bar{P}_{22}\xi(\tau + \Delta\tau) &= \bar{X}_2 - M_\alpha/U^2; \end{aligned} \tag{6}$$

$M(\alpha)$ has been replaced by $M_p\alpha(\tau + \Delta\tau) + M_\alpha$, where

$$M_p = \begin{cases} 1 & \text{for } \bar{\alpha} < \alpha_f \text{ and } \alpha_f + \delta < \bar{\alpha}, \\ M_f & \text{otherwise}, \end{cases} \tag{7}$$

and M_α is given by

$$M_\alpha = \begin{cases} M_0 - \alpha_f & \text{for } \bar{\alpha} < \alpha_f, \\ M_0 - M_f\alpha_f & \text{for } \alpha_f \leq \bar{\alpha} \leq \alpha_f + \delta, \\ M_0 - \alpha_f + \delta(M_f - 1) & \text{for } \alpha_f + \delta < \bar{\alpha}, \end{cases} \tag{8}$$

where $\bar{\alpha}$ is an estimate of α which is obtained by linear extrapolation between τ and $\tau + \Delta\tau$. The terms $\bar{P}_{11}$, $\bar{P}_{12}$, $\bar{P}_{21}$, $\bar{P}_{22}$, $\bar{X}_1$ and $\bar{X}_2$ are extremely lengthy and are given in Appendix A; however, what is of significance is that the $\bar{P}$ terms are independent of τ, and the $\bar{X}$ terms are functions of α and ξ at time τ, $\tau - \Delta\tau$ and $\tau - 2\Delta\tau$ only. Hence, the solution of equations (6), via inversion of the $\bar{P}$ matrix, yields the values of α and ξ at time $\tau + \Delta\tau$ in terms of α and ξ at time τ.

The procedure for solving equations (1) with a cubic nonlinearity was a little different. In this case, equations (1) were written in difference form as

$$\begin{aligned} \bar{P}_{11}\alpha(\tau + \Delta\tau) + \bar{P}_{12}\xi(\tau + \Delta\tau) &= \bar{X}_1, \\ [\bar{P}_{21} + \beta_1 U^{-2}]\alpha(\tau + \Delta\tau) + \bar{P}_{22}\xi(\tau + \Delta\tau) &= \bar{X}_2 - \bar{\beta}, \end{aligned} \tag{9}$$

where

$$\bar{\beta} = (\beta_0 + \beta_2\alpha^2(\tau + \Delta\tau) + \beta_3\alpha^3(\tau + \Delta\tau))/U^2,$$

and the terms $\bar{P}_{11}$, $\bar{P}_{12}$, $\bar{P}_{21}$, $\bar{P}_{22}$, $\bar{X}_1$ and $\bar{X}_2$ are again given in Appendix A. Because of

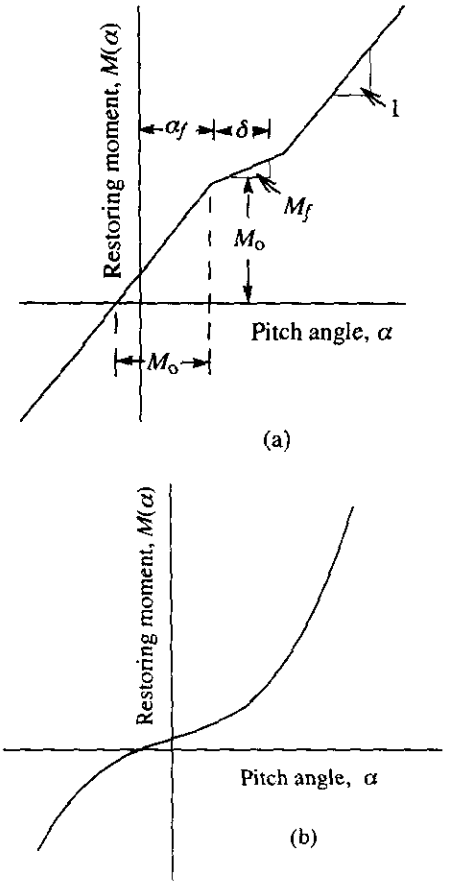

Figure 2. Schematic of the structural non-linearities: (a) bilinear stiffness; (b) cubic stiffness.

the terms involving $\alpha^2(\tau + \Delta\tau)$ and $\alpha^3(\tau + \Delta\tau)$ on the right-hand side of these equations, it is clear that $\alpha(\tau + \Delta\tau)$ and $\xi(\tau + \Delta\tau)$ cannot be obtained via simple matrix inversion, as was the case with the bilinear nonlinearity; instead $\alpha(\tau + \Delta\tau)$ and $\xi(\tau + \Delta\tau)$ were obtained from equation (9) using a Newton–Raphson technique.

One problem with using Houbolt's finite difference scheme occurs during the initial time step, $\tau = 0$; this is because Houbolt's finite difference method requires values of α and ξ at times $\tau - 2\Delta\tau$, $\tau - \Delta\tau$ and τ in order to determine the respective values at $\tau + \Delta\tau$. However, as previously shown by the authors (Price *et al.* 1993) this difficulty is overcome by using a Taylor's series expansion at $\tau = 0$ to give appropriate values of α and ξ at times $\tau - 2\Delta\tau$ and $\tau - \Delta\tau$.

2.2. Describing Function Method

In addition to the finite difference analysis, the nonlinear equations were also solved using a describing function method as discussed in this section.

The describing function technique is a method of obtaining an equivalent linear system, such that traditional aeroelastic methods of analysis can be employed. A describing function for a bilinear stiffness is given by Lee & Tron (1989), obtained using the method of Laurenson *et al.* (1986). However, this describing function is strictly applicable only where there is no preload. If a preload is applied, as in the

general case presented here, then the airfoil does not oscillate about the zero DC condition; instead, the airfoil pitch motion is of the form

$$\alpha(\tau) = B + A \sin \omega\tau.$$

To account for this DC offset a *dual-input describing function* technique must be used, as discussed by Gelb & Vander Velde (1968), which results in a DC component for the describing function. The dual-input describing function is given by

$$N = N_B + N_A \sin \omega\tau + N_C \cos \omega\tau,$$

and considering only the fundamental components of the restoring moment response, the following expressions for N_A, N_B and N_C are obtained

$$N_B = \frac{1}{2\pi}\int_{-\pi}^{\pi} M \, \mathrm{d}(\omega\tau), \qquad N_A = \frac{1}{\pi}\int_{-\pi}^{\pi} M \sin \omega\tau \, \mathrm{d}(\omega\tau)$$

and

$$N_C = \frac{1}{\pi}\int_{-\pi}^{\pi} M \cos \omega\tau \, \mathrm{d}(\omega\tau).$$

Evaluating the above integrals for the bilinear stiffness, accounting for the discontinuous nature of M, gives (after considerable algebra)

$$\begin{aligned} N_B &= A[(M_0 + M_f\delta/2)/A - (\gamma + \beta)/2 - (1 - M_f)g(\gamma) + (1 - M_f)g(\beta)], \\ N_A &= A[1 + (1 - M_f)(f(\gamma) - f(\beta))] \quad \text{and} \quad N_C = 0 \end{aligned} \tag{10}$$

where

$$f(x) = \begin{cases} 1/\pi(\sin^{-1}x + x(1 - x^2)^{1/2}) & \text{for } |x| < 1, \\ -1/2 & \text{for } x \le -1, \\ 1/2 & \text{for } x \ge 1, \end{cases} \tag{11}$$

$$g(x) = \begin{cases} 1/\pi(x \sin^{-1} x + (1 - x^2)^{1/2}) & \text{for } |x| \le 1, \\ |x|/2 & \text{for } |x| > 1, \end{cases} \tag{12}$$

$\gamma = (\alpha_f - B)/A$ and $\beta = (\alpha_f + \delta - B)/A$.

For the cubic nonlinearity, evaluation of the dual-input describing function is somewhat easier, as $M(\alpha)$ is continuous over the range of integration. The appropriate describing function is given by

$$\begin{aligned} N_B &= B[\beta_0/B + \beta_1 + \beta_2 B + \beta_3 B^2 + \tfrac{1}{2}A^2(\beta_2/B + 3\beta_3)], \\ N_A &= A[\beta_1 + 2\beta_2 B + 3\beta_3 B^2 + \tfrac{3}{4}\beta_3 A^2] \quad \text{and } N_C = 0. \end{aligned} \tag{13}$$

Once the appropriate describing function has been obtained, the method of solution using the describing function approach is relatively straightforward. In equation (1) the nonlinear term, $M(\alpha)$, is replaced by the describing function, given by either equation (10) or (13); however, the describing function depends on the amplitude of oscillation A and B, and thus, an iterative approach is required. First, it should be realised that there is no steady external moment, aerodynamic or otherwise, acting on the airfoil, hence, there can be no steady component to the restoring moment, or N_B must be equal to zero. Hence, in the iterative procedure a value of A is initially assumed, then by setting $N_B = 0$ the value of B is obtained, and so the equivalent linear stiffness given by the describing function is now known. From this point on the equations are solved using standard linear aeroelastic techniques, in this case the U–g method (Fung 1955)

was employed to determine the required value of U to give simple harmonic motion (which will be of amplitude equal to the assumed value of A). The above procedure is repeated for different values of A, and the variation of A and B with U is then obtained.

3. RESULTS AND DISCUSSION

The nonlinear equations for the airfoil plunge and pitch response have been solved using both the finite difference and describing function methods for a range of airfoil parameters. Only a sample of the results obtained will be presented here, and unless otherwise stated all are for $\bar{\omega} = 0{\cdot}2$, $\mu = 100$, $a_h = -0{\cdot}5$, $x_\alpha = 0{\cdot}25$, $r_\alpha = 0{\cdot}5$ and $\zeta_\alpha = \zeta_\xi = 0$.

In all cases in this paper the nondimensional air-speed, U, is presented normalized with respect to U^*, where U^* is defined as the linear flutter velocity. This was obtained by removing the structural nonlinearity [$M(\alpha)$ in equation (1) is replaced by α] and then increasing U in the finite difference method until divergent oscillations of α and ξ occurred. This was also checked using a standard U–g analysis and essentially the same values of U^* were obtained—to some extent this verified the finite difference method and computer code employed in the nonlinear calculations.

Figure 3 shows a typical bifurcation diagram of the pitch response for a cubic nonlinearity with no preload as a function of air-speed; results obtained using both the finite difference method and the describing function technique are presented. The finite difference results show the value of α when $\alpha' = 0$. If two points occur at one velocity this suggests that the motion is period-one, and four points suggests period-two;† hence, for period-one motion the value of α shown in the figure represents the magnitude of the limit cycle oscillation, LCO. It should be realised that the finite difference solution may possibly be dependent on the particular set of initial conditions for the airfoil (thus, this bifurcation diagram is particular to the set of initial conditions given in the figure caption); this will become more apparent in subsequent figures.

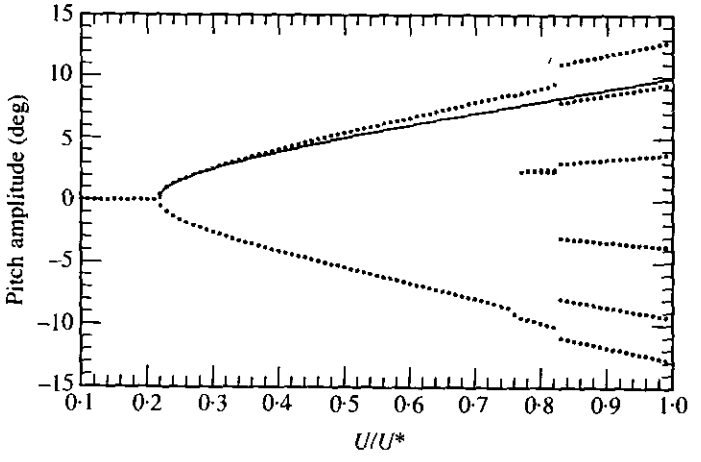

Figure 3. Comparison of the limit cycle amplitude obtained via the finite difference and describing function methods for the cubic nonlinearity; $\bar{\omega} = 0{\cdot}2$, $\mu = 100$, $a_h = -0{\cdot}5$, $r_\alpha = 0{\cdot}5$, $x_\alpha = 0{\cdot}25$, $\zeta_\alpha = 0{\cdot}0$, $\zeta_\xi = 0{\cdot}0$, $\beta_0 = 0{\cdot}0$/rad, $\beta_1 = 0{\cdot}1$/rad, $\beta_2 = 0{\cdot}0$/rad, $\beta_3 = 40{\cdot}0$/rad. ●, Finite difference method for $\alpha(0) = 7{\cdot}0°$, $\alpha'(0) = \xi(0) = \xi'(0) = 0$; —, describing function method.

† The period number of the response was verified using a spectral analysis of the time signal.

Because there is no preload for this case ($\beta_0 = 0$), the period-one motion is symmetrical about the $\alpha = 0$ axis. In the region $0{\cdot}76 \leq U/U^* \leq 0{\cdot}83$ approximately, this symmetry is lost; however, a different set of initial conditions will produce the exact mirror image about the $\alpha = 0$ axis.

The results presented in Figure 3 obtained using the describing function method show the value of A as a function of air-speed (because there is no preload, $B = 0$); the describing function solution does not require the initial conditions to be specified, and thus the describing function solution shown is good for any set of initial conditions, not just those given in the figure caption.

It can be seen that in this case both the finite difference and describing function solutions indicate a supercritical Hopf bifurcation at $U/U^* = 0{\cdot}22$, giving a period-one LCO. Furthermore, for $0{\cdot}22 \leq U/U^* \leq 0{\cdot}5$ approximately, the describing function and finite difference methods predict essentially the same magnitude of LC motion. However, as U/U^* increases, the describing function method gives an increasingly smaller prediction for the magnitude of the limit cycle (LC) motion compared with the finite difference solution. Most probably this disagreement at the higher values of U/U^* is because the describing function assumes a small nonlinearity, which in the case of a cubic nonlinearity becomes less admissible as the amplitude of vibration increases.

At $U/U^* = 0{\cdot}76$ the finite difference solution undergoes a further bifurcation to give period-two motion, and a final bifurcation is obtained at $U/U^* = 0{\cdot}83$ giving another periodic solution. Because the describing function used in this analysis assumes period-one motion, it is not capable of predicting the bifurcations at higher air-speeds.

A similar set of results for the bilinear nonlinearity is shown in Figure 4. However, in this case the finite difference solution, for this particular set of initial conditions, predicts that the initial loss of stability at $U/U^* = 0{\cdot}75$ is via a subcritical Hopf bifurcation and, furthermore, it results in a period-two motion. This is followed by a restabilization at $U/U^* = 0{\cdot}8$, and finally by the onset of period-one motion at $U/U^* = 0{\cdot}83$. Thus, it is clear that there is a region of period-two LC motion for velocities less than those required for the main body of period-one LC motion. Although not immediately apparent, closer examination of Figure 4 shows that the

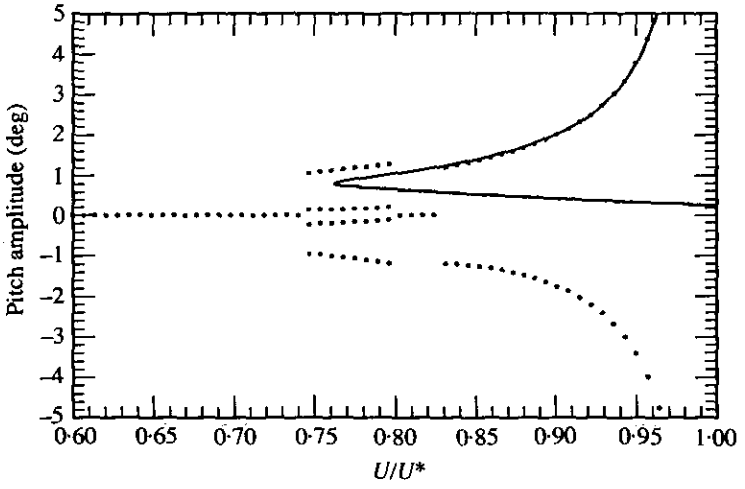

Figure 4. Comparison of the limit cycle amplitude obtained via the finite difference and describing function methods for the bilinear nonlinearity; $\bar{\omega} = 0{\cdot}2$, $\mu = 100$, $a_h = -0{\cdot}5$, $r_\alpha = 0{\cdot}5$, $x_\alpha = 0{\cdot}25$, $\zeta_\alpha = 0{\cdot}0$, $\zeta_\xi = 0{\cdot}0$, $\alpha_f = 0{\cdot}25°$, $\delta = 0{\cdot}5°$, $M_0 = 0{\cdot}25°$, $M_f = 0{\cdot}05$/rad. ●, Finite difference method for $\alpha(0) = -1{\cdot}0°$, $\alpha'(0) = \xi(0) = \xi'(0) = 0$; —, describing function method.

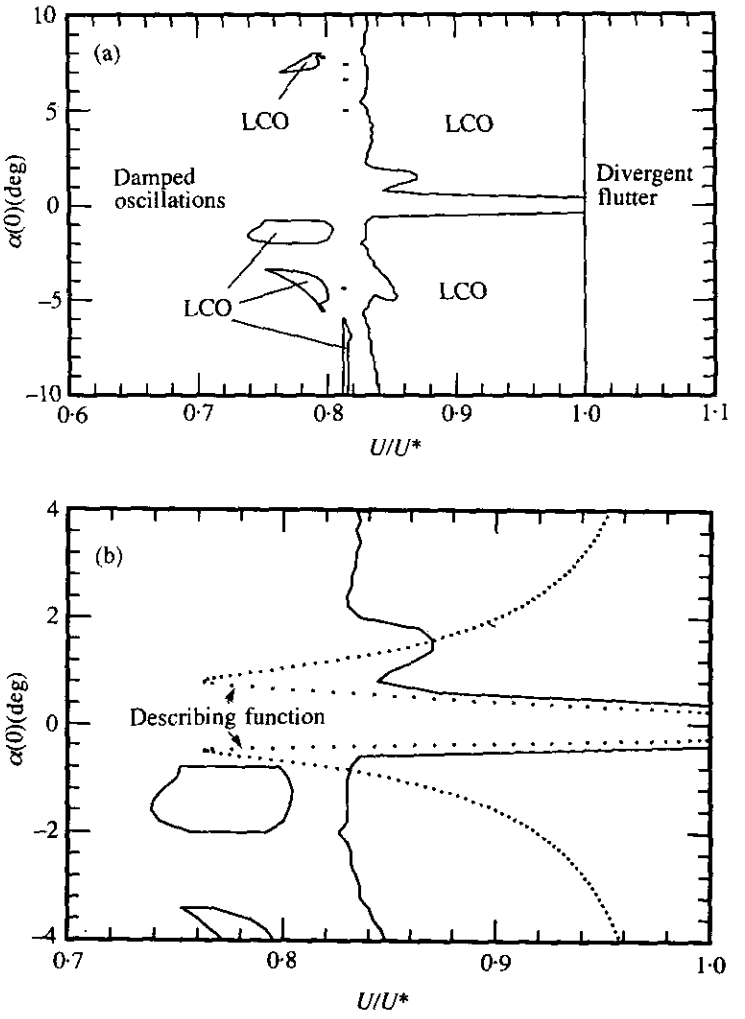

Figure 5. Two-dimensional section of the basin of attraction for LC motion of the bilinear nonlinearity obtained via the finite difference method; $\bar{\omega} = 0{\cdot}2$, $\mu = 100$, $a_h = -0{\cdot}5$, $r_\alpha = 0{\cdot}5$, $x_\alpha = 0{\cdot}25$, $\zeta_\alpha = 0{\cdot}0$, $\zeta_\xi = 0{\cdot}0$, $\alpha_f = 0{\cdot}25°$, $\delta = 0{\cdot}5°$, $M_0 = 0{\cdot}25°$, $M_f = 0{\cdot}05$/rad, $\alpha'(0) = \xi(0) = \xi'(0) = 0$. (a) General view; (b) enlarged view for a smaller region of $\alpha(0)$ and U/U^* plus; ●, the describing function solution.

finite difference solution is not symmetric about the $\alpha = 0$ axis; this is due to the small preload on the airfoil in this case.

The describing function solution gives two values of A (A_1 and A_2) for each value of U/U^*; furthermore, because there is a preload, in this case B is nonzero. Hence, what is presented in the figure is $B + A_1$ and $B + A_2$. Although not proven because of the non-analytical nature of the bilinear nonlinearity, after comparison with the finite difference solution presented in Figure 4 and other results presented in Figure 5, it is apparent that the larger value of A shown in Figure 4 represents a stable LCO, while the smaller value represents an unstable LCO. The unstable LCO gives a dividing line between stable and unstable motion: for $\alpha(0)$ less than this line the subsequent motion tends back to the stable equilibrium condition, and for $\alpha(0)$ greater than this line the subsequent motion tends towards the stable LCO.

The finite difference and describing function solutions presented in Figure 4 do not agree on the value of U/U^* at which instability first occurs, but once the period-one

motion commences the describing function method gives excellent agreement with the finite difference solution. As the amplitude of vibration increases, the effective nonlinearity of the bilinear stiffness decreases, in contrast to the cubic nonlinearity presented in Figure 3 and, hence, better agreement is obtained between the finite difference and describing function methods at higher values of U/U^*.

If the finite difference solution is repeated for the same airfoil with exactly the same nonlinearity as used for the results of Figure 4, but with different initial conditions for the airfoil, then it is found that whether or not LC motion occurs is very dependent on the particular initial conditions. This is indicated in Figure 5(a), where a two-dimensional section of the "basin of attraction" for LC motion is shown. The complete basin of attraction is five-dimensional, the dimensions being $\alpha(0)$, $\alpha'(0)$, $\xi(0)$, $\xi'(0)$ and U/U^*, but the two-dimensional section shown is for constant $\alpha'(0)$, $\xi(0)$ and $\xi'(0)$. As shown in the figure, there are apparent "islands" of LC motion below the main body of LC motion for some values of $\alpha(0)$; it is one of these islands of instability which gives the period-two motion for $0{\cdot}75 \leq U/U^* \leq 0{\cdot}83$ shown in Figure 4. This is in agreement with what the authors (Price *et al.* 1993) previously found with a free-play nonlinearity. For both the free-play and bilinear nonlinearities the LC motion in the islands of instability is period-two; hence, it is not surprising that the agreement between the finite difference and describing function solutions in these islands is not as good as elsewhere.

As shown in Figure 5(a), for small initial values of $\alpha(0)$, typically in the range $-0{\cdot}5° \leq \alpha(0) \leq 0{\cdot}5°$ instability is not obtained for $U/U^* \leq 1$. Qualitatively, this is in agreement with the unstable branch of the describing function solution presented in Figure 4. An enlarged view of the results for small $\alpha(0)$ shown in Figure 5(a) is given in Figure 5(b), where the describing function solution from Figure 4 is superimposed on the results—in Figure 5(b) the solutions $B - A_1$ and $B - A_2$ are presented in addition to $B + A_1$ and $B + A_2$ which are shown in Figure 4. As shown, there is reasonable, but not exact, agreement between the unstable LCO branch of the describing function method and the finite difference solution. Quite possibly the agreement between these two solutions for the unstable LCO motion could be improved if the finite difference solution were given for other values of $\alpha'(0)$, $\xi(0)$ and $\xi'(0)$.

Although not presented here, the LCO basin of attraction for the cubic nonlinearity is also strongly dependent on the initial conditions of the airfoil.

As previously observed by the authors for an airfoil with a free-play nonlinearity (Price *et al.* 1993), it was found that with the present nonlinearities, and for some airfoil parameters, no matter how long the finite difference time integration was allowed to run, the solution never converged to either a LCO or stable fixed point. An example of this is shown in Figure 6, where is it is clear that after a considerable period of time neither the pitch nor the plunge motion has reached either a steady limit cycle or an equilibrium position. This suggests the possibility of chaotic motion for this set of parameters (Thompson & Stewart 1986). This is further supported by the bifurcation diagram of Figure 7, which gives the value of α for $\alpha' = 0{\cdot}0$ as a function of U/U^* for the same airfoil as the results of Figure 6. It is clear that there is a significant range of velocity, $0{\cdot}3 \leq U/U^* \leq 0{\cdot}5$ approximately, where there appears to be a very large number of points in the bifurcation diagram at any particular velocity, suggesting non-periodic motion. Interestingly, as the velocity is increased beyond this nonperiodic region and approaches the divergent flutter condition, the airfoil motion goes from being nonperiodic (probably chaotic) to period-four, then period-two and finally period-one. A further indicator of chaos is the Poincaré section, and an example of this for $U/U^* = 0{\cdot}4$ is shown in Figure 8. It is clear that there is an extremely large number

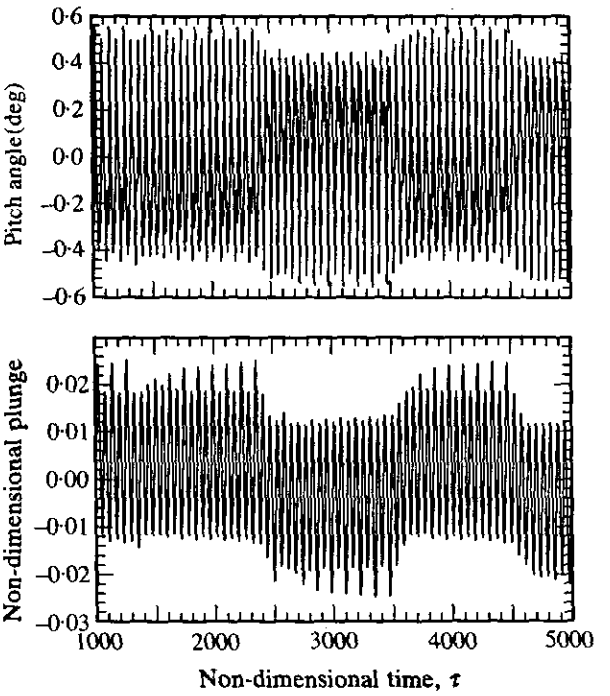

Figure 6. Time history of the airfoil pitch and plunge motion for the bilinear nonlinearity; $\bar{\omega} = 0{\cdot}2$, $\mu = 100$, $a_h = -0{\cdot}5$, $r_\alpha = 0{\cdot}5$, $x_\alpha = 0{\cdot}25$, $\zeta_\alpha = 0{\cdot}0$, $\zeta_\xi = 0{\cdot}0$, $\alpha_f = -0{\cdot}25°$, $\delta = 0{\cdot}5°$, $M_0 = -0{\cdot}0025°$, $M_f = 0{\cdot}01$/rad, $\alpha(0) = 3{\cdot}0°$, $\alpha'(0) = \xi(0) = \xi'(0) = 0$, $U/U^* = 0{\cdot}4$.

of points in the Poincaré section, indicating nonperiodic motion, but also that there is some "structure" to the Poincaré section indicating that the motion is not random but is most probably chaotic.

This apparently chaotic motion could also be obtained with the cubic nonlinearity, as indicated by both the bifurcation diagram and Poincaré section in Figure 9.

Although the bifurcation diagrams of Figures 7 and 9(a), the time histories of Figure 6, and the Poincaré sections of Figures 8 and 9(b), as well as spectral density plots not

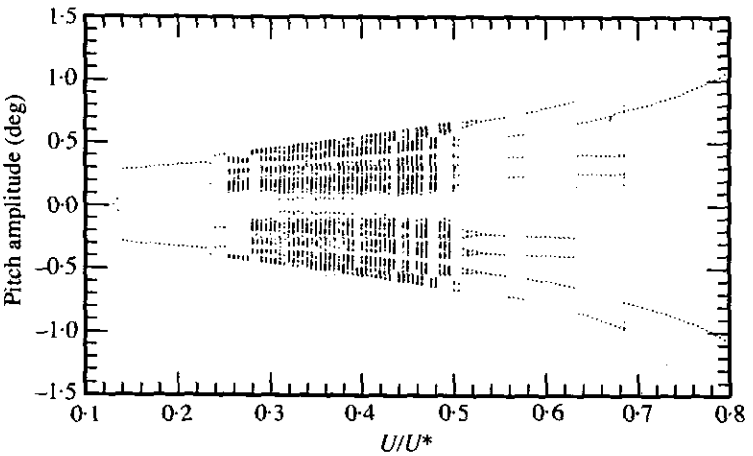

Figure 7. Bifurcation diagram showing α for $\alpha' = 0$ as a function of U/U^* for the same airfoil as Figure 6; $\alpha(0) = 3{\cdot}0°$, $\alpha'(0) = \xi(0) = \xi'(0) = 0$.

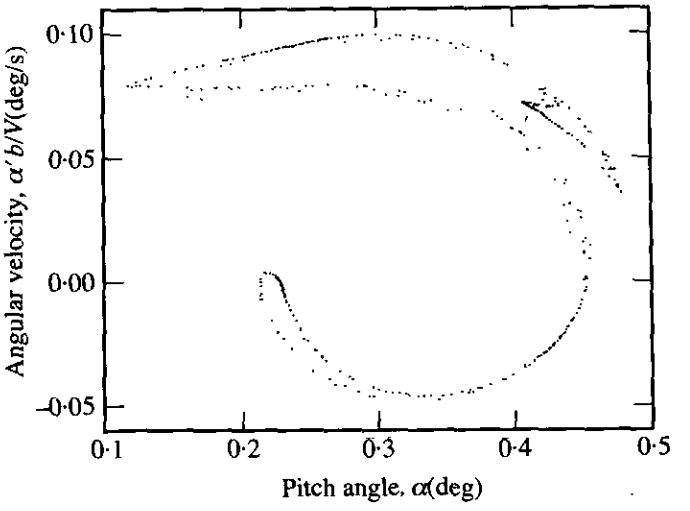

Figure 8. Poincaré section for the same airfoil as Figure 6 at $U/U^* = 0{\cdot}4$; $\alpha(0) = 3{\cdot}0°$, $\alpha'(0) = \xi(0) = \xi'(0) = 0$.

presented here, are all indicative of chaos, they do not give an absolute proof of chaos as discussed by Moon (1987). A far more definitive method is the use of Lyapunov exponents (Moon 1987), which give a measure of the rate of divergence or convergence of nearby orbits in phase space; a positive Lyapunov exponent indicating a chaotic system. In principle, the Lyapunov exponents can be calculated for any known time history using the algorithm developed by Wolf *et al.* (1985); however, previous experience (Mureithi *et al.* 1994) has indicated that there are practical problems in applying this algorithm and interpreting the results, as also mentioned by Moon (1987). However, because of the analytical nature of the cubic nonlinearity, it is possible to calculate the Lyapunov spectrum directly from the differential equations. Space limitations do not permit full details of this to be presented here, and only the overall details are given.

First, equations (1) are differentiated twice to remove the integrals in the aerodynamic terms. These equations can then be written as eight first-order differential equations

$$\{x'\} = f(\{x\}),$$

where

$$\{x\} = \{\alpha''', \xi''', \alpha'', \xi'', \alpha', \xi', \alpha, \xi\}^T,$$

and $f(\{x\})$ is a series of rather long expressions not given here for the sake of brevity. The Jacobian of the function $f(\{x\})$ is evaluated to enable linearization of the equations about the fixed point $\{\bar{x}\}$. Then, using the algorithm given by Wolf *et al.* (1985) for calculation of the Lyapunov spectrum from differential equations, based on techniques developed by Benettin *et al.* (1980) and Shimada & Nagashima (1979), the complete Lyapunov spectrum was calculated at a number of different velocities for the bifurcation diagram of Figure 9(a). In those cases where the bifurcation diagram indicated periodic motion, all of the Lyapunov exponents were either negative or zero, in agreement with the bifurcation diagram. However, for $U/U^* = 0{\cdot}47$, in the middle of the apparently chaotic region of the bifurcation diagram shown in Figure 9(a), a positive Lyapunov exponent of 0·01 was calculated, indicating that the system is "mildly" chaotic, which is in agreement with the previous conclusion. Hence, for the

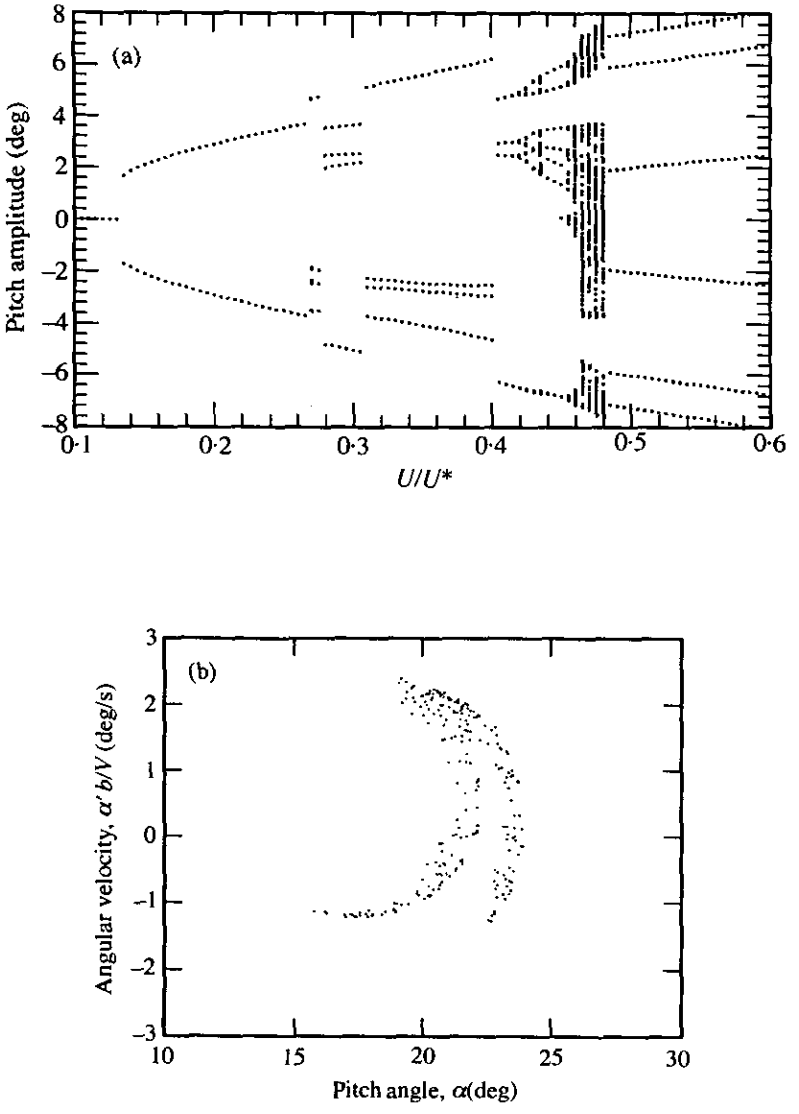

Figure 9. (a) Bifurcation diagram showing α for $\alpha' = 0$ as a function of U/U^*; (b) Poincaré section for $U/U^* = 0{\cdot}475$, for the airfoil with a cubic nonlinearity; $\alpha(0) = 3{\cdot}0°$, $\alpha'(0) = \xi(0) = \xi'(0) = 0$, $\bar{\omega} = 0{\cdot}2$, $\mu = 200$, $a_h = -0{\cdot}5$, $r_\alpha = 0{\cdot}5$, $x_\alpha = 0{\cdot}25$, $\zeta_\alpha = 0{\cdot}0$, $\zeta_\xi = 0{\cdot}0$, $\beta_0 = 0{\cdot}0$/rad, $\beta_1 = 0{\cdot}01$/rad, $\beta_2 = 0{\cdot}0$/rad, $\beta_3 = 50{\cdot}0$/rad.

cubic nonlinearity it can now be stated quite categorically that the sytem is indeed chaotic for a limited range of parameters. Although such a definite statement cannot be made for the bilinear nonlinearity, by inference it can be said that the motion in the bifurcation diagram of Figure 7 is also chaotic for $0{\cdot}22 \leq U/U^* \leq 0{\cdot}48$, approximately.

Proving that chaos can occur for the cubic nonlinearity shows that the cause of this chaotic motion is not the discontinuous nature of the stiffness associated with a bilinear nonlinearity, but that chaos can occur for gradual variations in stiffness—as is the case with a cubic nonlinearity.

One significant difference between the bifurcation diagrams for the cubic and bilinear nonlinearities can be seen by comparing Figures 7 and 9(a). For the bilinear nonlinearity, shown in Figure 7, there is a period-doubling route to chaos if the chaotic

region is approached as velocity decreases; for the cubic nonlinearity there is also a period doubling route to chaos but this time with increasing velocity, see Figure 9(a). One possible explanation for this behaviour is the different manner in which the nonlinearities behave as the amplitude of oscillation increases. The cubic nonlinearity becomes more nonlinear as the amplitude of oscillation increases, corresponding to increasing velocity, while the bilinear nonlinearity becomes more nonlinear as the amplitude of oscillation decreases, corresponding to a decrease in velocity.

All of the results presented so far have been for zero structural damping, but it is of interest to see what the effect of structural damping is on the aeroelastic response of the airfoil. Figure 10 shows three bifurcation diagrams for the airfoil with a bilinear nonlinearity and the same parameters as Figure 6, but with three different levels of structural damping. The bifurcation diagram shown in Figure 10(a), with 2% critical structural damping, is very similar to that shown in Figure 7 with zero structural damping, suggesting that the airfoil motion is still chaotic. Increasing the structural damping to 5% of critical reduces the regions of apparently chaotic motion as shown in Figure 10(b), and for 10% of critical damping it is clear that the airfoil motion is now periodic as shown in Figure 10(c). Thus, it seems that a reasonably large amount of structural damping can eliminate the chaotic response of the airfoil, but that chaotic motion can still occur for small amounts of structural damping. Results were also obtained with structural damping for the cubic nonlinearity, showing a similar trend to that presented in Figure 10.

As mentioned in the Introduction, a very similar analysis to that presented here was also undertaken by Zhao & Yang (1990). They investigated the effect of the elastic axis position, denoted by $a_h b$ in Figure 1, on the dynamic response of an airfoil with a cubic nonlinearity. Superficially, the results obtained by Zhao & Yang (1990) are very similar to those presented here. However, one significant difference is that Zhao & Yang (1990) found that chaos, or what they inferred to be chaos from their phase plane plots, would only occur for velocities in excess of that required for static divergence. The present results, all of which are with the elastic axis coincident with the aerodynamic center, $a_h = -0{\cdot}5$ [hence, as shown for example by Fung (1955), no divergence is possible], are obviously contradictory to this. Although the present authors only became aware of Zhao & Yang's work very late in the preparation of this manuscript they were intrigued by this obvious contradiction, and thus, they attempted to duplicate the results of Zhao & Yang for some cases where the elastic axis was aft of the aerodynamic centre. In fact, $a_h = 0{\cdot}2$ was chosen, which corresponds to an elastic axis position where Zhao & Yang (1990) present a large number of phase plane plots showing both a period-two response and chaos for a narrow range of velocities (the other airfoil parameters were modified such that they were equivalent to those given by Zhao & Yang). Surprisingly, the authors found that with the elastic axis at this position, after the initial Hopf bifurcation the response was purely period-one for velocities up to a far greater value than those quoted by Zhao & Yang. To ensure that the authors had not misunderstood something in Zhao & Yang's paper, the analysis was repeated using quasi-static aerodynamics—hence, the two sets of equations are identical—and, as expected, virtually identical results to those of Zhao & Yang (1990) were obtained. Thus, it appears that the dynamic response of the airfoil is quite sensitive to the manner in which the aerodynamic forces is represented. In this respect, the authors are firmly convinced that their unsteady representation of the aerodynamics is far more accurate than the quasi-static representation of Zhao & Yang (1990), and thus, suggest that the dynamic responses presented here are more realistic than those suggested by Zhao & Yang (1990).

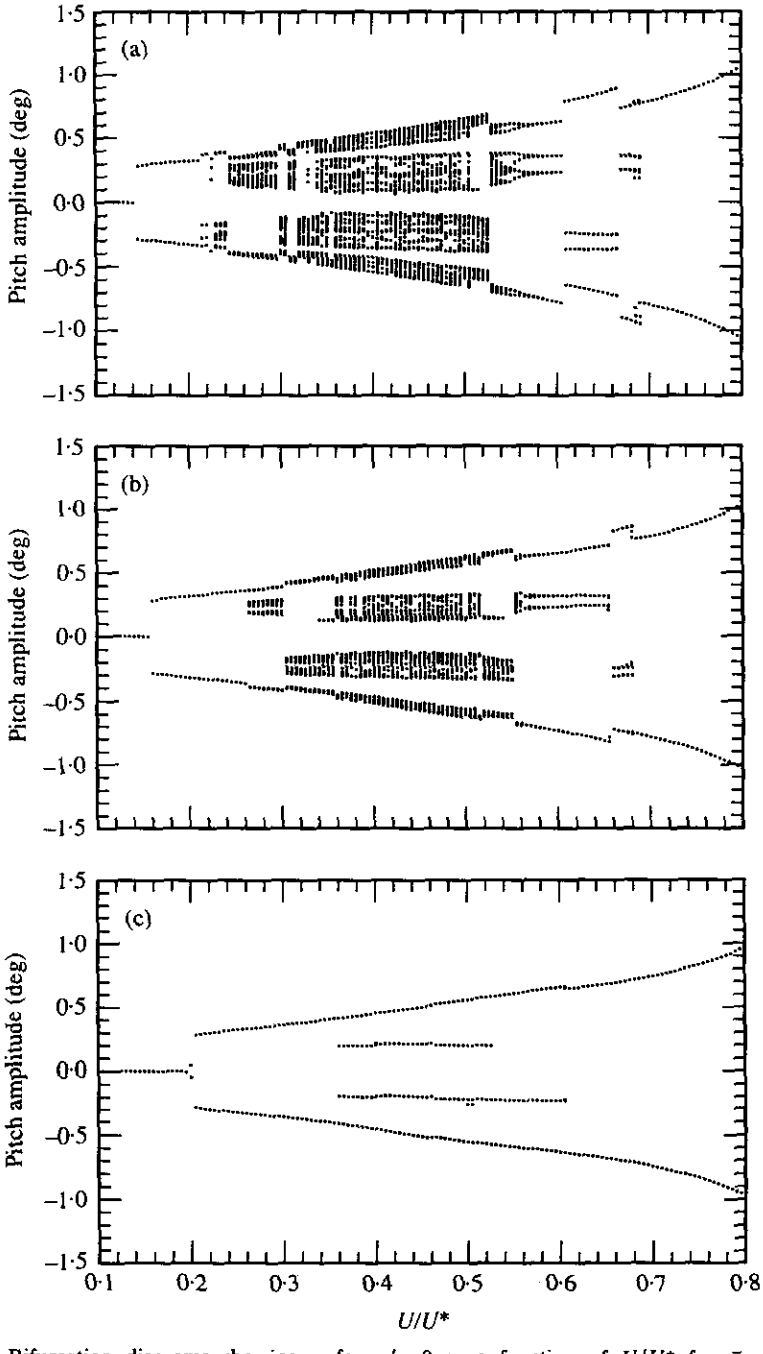

Figure 10. Bifurcation diagrams showing α for $\alpha' = 0$ as a function of U/U^* for $\bar{\omega} = 0{\cdot}2$, $\mu = 100$, $a_h = -0{\cdot}5$, $r_\alpha = 0{\cdot}5$, $x_\alpha = 0{\cdot}25$, $\alpha_f = -0{\cdot}25°$, $\delta = 0{\cdot}5°$, $M_0 = -0{\cdot}0025°$, $M_f = 0{\cdot}01$/rad, $\alpha(0) = 3{\cdot}0°$, $\alpha'(0) = \xi(0) = \xi'(0) = 0$. (a) $\zeta_\alpha = \zeta_\xi = 0{\cdot}02$; (b) $\zeta_\alpha = \zeta_\xi = 0{\cdot}05$; (c) $\zeta_\alpha = \zeta_\xi = 0{\cdot}1$.

4. CONCLUSIONS

The aeroelastic response of a two-degree-of-freedom airfoil in incompressible flow with a structural nonlinearity in pitch has been analysed. Two different types of nonlinearity have been considered; these being bilinear and cubic nonlinearities. The resulting equations of motion have been solved using both a finite difference method and a dual-input describing function technique.

For both a bilinear and hardening cubic nonlinearity, limit cycle oscillations are obtained at velocities well below the divergent flutter boundary. In those cases where the LCO is period-one there is good agreement between the finite difference and describing function solutions. However, by its very nature, the describing function solution used here is not capable of predicting the higher order periodic motion suggested by the finite difference solution for some parameters.

In some cases, most notably where the airfoil was subject to small preloads, the finite difference solution never settled down to either an equilibrium position or a steady limit cycle. An analysis of the Poincaré sections and spectral density plots suggested that in these cases the motion is chaotic. This was confirmed for the cubic nonlinearity via the use of Lyapunov exponents, it being shown that in those regions where the system appeared to be chaotic a positive Lyapunov exponent existed. The proof of chaos for the cubic nonlinearity is significant, because it establishes that the cause of chaos is not the discontinuous nature of the restoring moment associated with a bilinear nonlinearity. The results presented here add to the list of cases where chaotic motion has been predicted for airfoils subject to either structural (Yang & Zhao 1988; Hauenstein *et al.* 1990; Zhao & Yang 1990; Tang & Dowell 1992a; Price *et al.* 1993) or aerodynamic (Tang & Dowell 1992b) nonlinearities.

ACKNOWLEDGEMENTS

The authors gratefully acknowledge the financial support of the Department of National Defence, the Institute for Aerospace Research and the Natural Sciences and Engineering Research Council of Canada. They would also like to acknowledge one of the anonymous reviewers of this paper who bought to their attention the paper of Zhao & Yang (1990).

REFERENCES

BENETTIN, G., GALGANI, L., GIORGILLI, A. & STRELCYN, J. M. 1980 Lyapunov characteristic exponents for smooth dynamical systems and for Hamiltonian systems; a method for computing all of them. Part 2: Numerical application. *Meccanica* **15**, 21–30.

BRIETBACH, E. 1977 Effect of structural nonlinearities on aircraft vibration and flutter. Presented at the 45th Structures and Materials AGARD Panel Meeting, Voss, Norway, AGARD Report 665.

DOWELL, E. H. & ILGAMOV, M. 1988 *Studies in Nonlinear Aeroelasticity.* New York: Springer-Verlag.

FUNG, Y. C. 1955 *An Introduction to the Theory of Aeroelasticity.* New York: John Wiley.

GELB, A. & VANDER VELDE, W. A. 1968 *Multiple-Input Describing Functions and Nonlinear System Design.* New York: McGraw-Hill.

HAUENSTEIN, A. J., LAURENSON, R. M., EVERSMAN, W., GALECKI, G., QUMEI, I. & AMOS, A. K. 1990 Chaotic response of aerosurfaces with structural nonlinearities. *Proceedings of the 31st AIAA/ASME/ASCE/AHS/ASC Structures, Structural Dynamics and Materials Conference*, pp. 1530–1539.

HAUENSTEIN, A. J., ZARA, J., EVERSMAN, W. & QUMEI, I. 1992 Chaotic and nonlinear dynamic

response of aerosurfaces with structural nonlinearities. *Proceedings of the 33rd AIAA/ASME/ASCE/AHS/ASC Structures, Structural Dynamics and Materials Conference, Part 4: Structural Dynamics II*, Dallas, pp. 2367–2375.

HOUBOLT, J. C. 1950. A recurrence matrix solution for the dynamic response of elastic aircraft. *Journal of Aeronautical Sciences*, **17** 540–550.

LAURENSON, R. M., HAUENSTEIN, A. J. & GUBSER, J. L. 1986 Effects of structural nonlinearities on limit-cycle response of aerodynamic surfaces. AIAA Paper 86-0899.

LEE, B. H. K. & DESROCHERS, J. 1987 Flutter analysis of a two-dimensional airfoil containing structural nonlinearities. National Research Council of Canada, Aeronautical Report LR-618, Ottawa, Canada.

LEE, B. H. K. & TRON, A. 1989 Effects of structural nonlinearities on flutter characteristics of the CF-18 aircraft. *Journal of Aircraft* **26**, 781–786.

MCINTOSH, S. C., REED, R. E. & RODDEN, W. P. 1981 Experimental and theoretical study of nonlinear flutter. *Journal of Aircraft* **18**, 1057–1063.

MOON, F. C. 1987 *Chaotic Vibration: An Introduction for Applied Scientists and Engineers*, New York: John Wiley.

MUREITHI, N. W., PAIDOUSSIS, M. P. & PRICE, S. J. 1994 The post-Hopf-bifurcation response of a loosely-supported cylinder in an array subjected to cross-flow. Part II: Theoretical model and comparison with experiments. *Journal of Fluids and Structures* **8**, 853–876.

PRICE, S. J., LEE, B. H. K. & ALIGHANBARI, H. 1993 An analysis of the post-instability behaviour of a two-dimensional airfoil with a structural nonlinearity. *Proceedings of the 34th AIAA/ASME/ASCE/AHS/ASC Structures, Structural Dynamics and Materials Conference*, pp. 1452–1460. Also *Journal of Aircraft* 1994, **31**, 1395–1401.

SHIMADA, I. & NAGASHIMA, T. 1979 A numerical approach to ergodic problem of dissipative dynamical systems. *Progress of Theoretical Physics* **61**, 1605–1616.

TANG, D. M. & DOWELL, E. H. 1992a Flutter and stall response of a helicopter blade with structural nonlinearity. *Journal of Aircraft* **29**, 953–960.

TANG, D. M. & DOWELL, E. H. 1992b Chaotic stall response of a helicopter rotor in forward flight. *Journal of Fluids and Structures* **6**, 311–336.

THOMPSON, J. M. T. & STEWART, H. B. 1986 *Nonlinear Dynamics and Chaos*. Chichester: John Wiley.

WOLF, A., SWIFT, J. B., SWINNEY, H. L. & VASTANO, J. A. 1985 Determining Lyapunov exponents from a time series. *Physica* **16D**, 285–317.

YANG, Z. C. & ZHAO, L. C. 1988 Analysis of limit cycle flutter of an airfoil in incompressible flow. *Journal of Sound and Vibration* **123**, 1–13.

ZHAO, L. C. & YANG, Z. C. 1990 Chaotic motions of an airfoil with nonlinear stiffness in incompressible flow. *Journal of Sound and Vibration* **138**, 245–254.

APPENDIX A: COEFFICIENTS IN EQUATIONS (6) AND (9)

The coefficients $\bar{P}_{11}$, $\bar{P}_{12}$, $\bar{P}_{21}$ and $\bar{P}_{22}$ in equations (6) and (9) are as follows:

$$\bar{P}_{11} = 2c_2/\Delta\tau^2 + 11c_4/(6\Delta\tau) + c_6, \qquad \bar{P}_{12} = 2c_1/\Delta\tau^2 + 11c_3/(6\Delta\tau) + c_5,$$

$$\bar{P}_{21} = 2d_2/\Delta\tau^2 + 11d_4/(6\Delta\tau) + d_6, \qquad \bar{P}_{22} = 2d_1/\Delta\tau^2 + 11d_3/(6\Delta\tau),$$

where the c_i and d_i terms are given by

$$c_1 = 1 + (1 - \tfrac{3}{4}\Delta\tau(a + c))/\mu, \qquad c_2 = x_\alpha - (a_h + \tfrac{3}{4}\Delta\tau(a + c)\bar{a}_h)/\mu,$$

$$c_3 = 2\zeta_\xi\bar{\omega}/U + 2l/\mu, \qquad c_4 = (1 + 2l\bar{a}_h - \tfrac{3}{4}(a + c)\Delta\tau)/\mu,$$

$$c_5 = (\bar{\omega}/U)^2, \qquad c_6 = 2l/\mu,$$

$$d_1 = [x_\alpha - a_h/\mu + \tfrac{3}{4}\Delta\tau(a + c)(\tfrac{1}{2} + a_h)/\mu]/r_\alpha^2,$$

$$d_2 = 1 + [\tfrac{1}{8} + a_h^2 + \tfrac{3}{4}\Delta\tau(a + c)\bar{a}_h(\tfrac{1}{2} + a_h)]/(\mu r_\alpha^2),$$

$$d_3 = -2l(\tfrac{1}{2} + a_h)/(\mu r_\alpha^2), \qquad d_6 = -2l(\tfrac{1}{2} + a_h)/(\mu r_\alpha^2),$$

$$d_4 = 2\zeta_\alpha/U + [\bar{a}_h - 2l\bar{a}_h(\tfrac{1}{2} + a_h) + \tfrac{3}{4}\Delta\tau(a + c)(\tfrac{1}{2} + a_h)]/(\mu r_\alpha^2).$$

The terms $\bar{X}_1$ and $\bar{X}_2$ in equations (6) and (9) are as follows:

$$\bar{X}_1 = x_{11}\alpha(\tau) + x_{13}\alpha(\tau - \Delta\tau) + x_{15}\alpha(\tau - 2\Delta\tau) + x_{12}\xi(\tau) + x_{14}\xi(\tau - \Delta\tau) + x_{16}\xi(\tau - 2\Delta\tau) + x_{17},$$

$$\bar{X}_2 = x_{21}\alpha(\tau) + x_{23}\alpha(\tau - \Delta\tau) + x_{25}\alpha(\tau - 2\Delta\tau) + x_{22}\xi(\tau) + x_{24}\xi(\tau - \Delta\tau) + x_{26}\xi(\tau - 2\Delta\tau) + x_{27},$$

where the x_{ij} terms are

$$x_{11} = 5c_2/\Delta\tau^2 + 18c_4/(6\Delta\tau), \qquad x_{12} = 5c_1/\Delta\tau^2 + 18c_3/(6\Delta\tau),$$

$$x_{13} = -4c_2/\Delta\tau^2 - 9c_4/(6\Delta\tau), \qquad x_{14} = -4c_1/\Delta\tau^2 - 9c_3/(6\Delta\tau),$$

$$x_{15} = c_2/\Delta\tau^2 + 2c_4/(6\Delta\tau), \qquad x_{16} = c_1/\Delta\tau^2 + 2c_3/(6\Delta\tau),$$

$$x_{17} = -2(L_0 - aI_b(\tau + \Delta\tau) - cI_d(\tau + \Delta\tau) - x_{17a}\lambda(\tau) + x_{17b}\lambda(\tau - \Delta\tau) - x_{17c}\lambda(\tau - 2\Delta\tau))/\mu,$$

$$x_{21} = 5d_2/\Delta\tau^2 + 18d_4/(6\Delta\tau), \qquad x_{22} = 5d_1/\Delta\tau^2 + 18d_3/(6\Delta\tau),$$

$$x_{23} = -4d_2/\Delta\tau^2 - 9d_4/(6\Delta\tau), \qquad x_{24} = -4d_1/\Delta\tau^2 - 9d_3/(6\Delta\tau),$$

$$x_{25} = d_2/\Delta\tau^2 + 2d_4/(6\Delta\tau), \qquad x_{26} = d_1/\Delta\tau^2 + 2d_3/(6\Delta\tau),$$

$$x_{27} = -(\tfrac{1}{2} + a_h)x_{17}/r_\alpha^2,$$

in which

$$x_{17a} = \tfrac{19}{24}\Delta\tau(ae^{-b\Delta\tau} + ce^{-d\Delta\tau}), \qquad x_{17b} = \tfrac{5}{24}\Delta\tau(ae^{-2b\Delta\tau} + ce^{-2d\Delta\tau}),$$

$$x_{17c} = \tfrac{1}{24}\Delta\tau(ae^{-3b\Delta\tau} + ce^{-3d\Delta\tau}),$$

$$L_0 = (-ae^{-b(\tau+\Delta\tau)} - ce^{-d(\tau+\Delta\tau)})[\xi'(0) + \bar{a}_h\alpha'(0) + \alpha(0)],$$

$$I_b(\tau + \Delta\tau) = e^{-b\Delta\tau}\{I_b(\tau) + \tfrac{1}{24}\Delta\tau[9\lambda(\tau) + 19\lambda(\tau - \Delta\tau)e^{-b\Delta\tau} - 5\lambda(\tau - 2\Delta\tau)e^{-2b\Delta\tau} + \lambda(\tau - 3\Delta\tau)e^{-3b\Delta\tau}]\},$$

$$I_d(\tau + \Delta\tau) = e^{-d\Delta\tau}\{I_d(\tau) + \tfrac{1}{24}\Delta\tau[9\lambda(\tau) + 19\lambda(\tau - \Delta\tau)e^{-d\Delta\tau} - 5\lambda(\tau - 2\Delta\tau)e^{-2d\Delta\tau} + \lambda(\tau - 3\Delta\tau)e^{-3d\Delta\tau}]\},$$

$$\lambda(\tau) = \xi''(\tau) + \bar{a}_h\alpha''(\tau) + \alpha'(\tau),$$

$$\alpha'(\tau + \Delta\tau) = \frac{1}{6\Delta\tau}[11\alpha(\tau + \Delta\tau) - 18\alpha(\tau) + 9\alpha(\tau - \Delta\tau) - 2\alpha(\tau - 2\Delta\tau)],$$

$$\alpha''(\tau + \Delta\tau) = \frac{1}{\Delta\tau^2}[2\alpha(\tau + \Delta\tau) - 5\alpha(\tau) + 4\alpha(t - \Delta\tau) - \alpha(\tau - 2\Delta\tau)],$$

and

$$\xi''(\tau + \Delta\tau) = \frac{1}{\Delta\tau^2}[2\xi(\tau + \Delta\tau) - 5\xi(\tau) + 4\xi(\tau - \Delta\tau) - \xi(\tau - 2\Delta\tau)].$$

APPENDIX B: NOMENCLATURE

A	sinusoidal amplitude in the describing function solution
B	DC amplitude in the describing function solution
a_h	nondimensional distance between elastic axis and mid-chord, see Figure 1
$\bar{a}_h$	$(1/2 - a_h)$
b	semi-chord
m	airfoil mass
M	nonlinear structural restoring moment
M_0	restoring moment at the start of the central bilinear stiffness, see Figure 2(a)
M_f	central stiffness term for the bilinear stiffness, see Figure 2(a)

N	describing function
N_A, N_C	oscillatory terms in the describing function
N_B	DC term in the describing function
p	nondimensional aerodynamic force in the plunge direction, Pb/V^2m
r	nondimensional aerodynamic pitching moment, Rb^2/V^2I_α
r_α	radius of gyration
U	nondimensional free-stream velocity, $V/b\omega_\alpha$
U^*	nondimensional linear flutter velocity
x_α	nondimensional distance from elastic axis to centre of mass, see Figure 1
α	pitch rotation of the airfoil
$\bar{\alpha}$	interpolated estimate of α, see equation (8)
α_f	see Figure 2(a)
β_i	terms in the cubic nonlinearity
δ	pitch angle for the central region of the bilinear stiffness, see Figure 2(a)
ζ_ξ, ζ_α	viscous damping ratios in plunge and pitch
μ	airfoil/air mass ratio, $m/\pi\rho b^2$
ξ	nondimensional plunge displacement, h/b
τ	nondimensional time, tV/b
ω_ξ, ω_α	radian frequencies in plunge and pitch
$\bar{\omega}$	frequency ratio, ω_ξ/ω_α